Ocean Waves Measurement and Analysis, Fifth International Symposium WAVES 2005, 3rd-7th, July, 2005. Madrid, Spain
Paper number: 46

BLOCKING OF PERIODIC AND RANDOM WAVES

Ketut Suastika [1] and Jurjen Battjes [2]

Abstract: This paper describes an experimental and modelling investigation of wave blocking. The modelling takes breaking-induced dissipation into account and consists of a WKB-solution for slowly varying waves away from the blocking region, which is matched to a uniformly valid expansion for the rapidly varying waves in the blocking region.

INTRODUCTION

Blocking of gravity surface waves by a counter current is a significant phenomenon in several river outfalls and tidal inlets around the world. Existing models for wave blocking typically are either dissipationless, with a uniformly-valid approximation in the vicinity of the blocking point including 100% reflection (e.g. Smith 1975), or they use a wave action balance with breaking-induced dissipation (e.g. Chawla and Kirby 1998, 2002; Suastika et al. 2000). Neither is satisfactory because the shortening and steepening of the waves in the approach to blocking usually gives rise to breaking (except for very low initial steepness), which is absent in the former category of models, whereas the solution on the basis of a wave action balance is in principle singular in the blocking point and therefore not valid in that region, although the dissipation plays a moderating role and so can save the situation to some extent.

In the present work, a model was developed that includes breaking-induced dissipation. This was included in a wave action balance equation for the slowly varying waves in the far field, in the approach to the blocking point, matched to a uniformly-valid approximation for the rapidly varying waves near the blocking point. The model has been elaborated both for periodic waves and for random waves.

EXPERIMENTS

A 40 m long flume was used, equipped with a wave generator at one end, with permeable wave damping material at the opposite end where also a flow of water could be let into the flume with controlled discharge. Large-scale turbulence and swirling motions in the

[1](Formerly at) Delft University of Technology, PO Box 5048, 2600 GA Delft, The Netherlands, k_suastika@yahoo.com
[2]Emeritus professor in Fluid Mechanics, Delft University of Technology, PO Box 5048, 2600 GA Delft, The Netherlands, j.battjes@ct.tudelft.nl

inflowing current were dampened by a honeycomb. At both ends the full flume width (0.8 m) and height (1.0 m) were available to the waves and the current, respectively, but with the aid of a vertical false wall and a false bottom the available width and height were reduced to 0.4 m and 0.7 m in the measurement section in the middle part of the flume.

Previous laboratory experiments of wave blocking have utilized a constant discharge and varied the cross-section to obtain a longitudinal gradient of mean longitudinal velocity, by placing an impermeable plane sloping bottom or a false vertical wall along a segment of the flume. We have designed and built a novel experimental arrangement in the present study, in which the flume cross-section is held constant but the discharge, and therefore the flow velocity, has a longitudinal variation, obtained by withdrawal of water through a perforated false bottom extending over 12 m (Suastika et al., 2000). The result is a virtually linear decrease of the discharge and of the cross-sectionally averaged flow velocity in this interval from a maximum at the upstream (down-wave) cross-section to zero at the downstream (up-wave) cross-section. Downstream from the measurement section with variable discharge a 20 m-long region exists where the discharge, and therefore the cross-sectionally averaged current velocity, is zero. In this stagnant region waves were generated by a piston-type wave generator with second-order control and automatic reflection absorption.

A MODEL FOR BLOCKING OF PERIODIC WAVES

In this chapter we present a linear model for the amplitude evolution of periodic gravity surface waves blocked by a collinear adverse current. The model essentially combines a linear ray approximation in the region far from the blocking point (far field) with a linear uniformly-valid approximation in the vicinity of the blocking point (near field). Wave energy dissipation is modelled both in the far field and in the near field.

Ray Approximation for the Far Field

The spatial evolution of the incident wave amplitude in the far field is represented by a wave action balance:

$$\frac{d}{dx}[(c_g + U)\frac{E}{\sigma}] + \frac{D}{\sigma} = 0. \tag{1}$$

In Eq. (1) E is the wave energy density, σ is the intrinsic wave frequency, c_g is the intrinsic wave group velocity, U is the mean current velocity and D is the rate of wave energy dissipation per unit area of bottom. Due to the current, the wave frequency is Doppler shifted, given as $\omega = \sigma + kU$, where ω is the wave frequency relative to the fixed bed and k is the wave number. The intrinsic group velocity c_g is given as $c_g = \partial\sigma/\partial k$.

Dissipation at Sidewalls and Bottom

Wave energy dissipation in the boundary layers at the sidewalls and at the perforated bottom is expressed in terms of an amplitude decay modulus (imaginary part of the wave number) μ. The corresponding expression for the energy dissipation rate is

$$D_b = 2\mu c_g E, \tag{2}$$

in which $\mu = \mu_w + \mu_p$, with μ_w the damping modulus for sidewall dissipation and μ_p the damping modulus for perforated bottom dissipation. The former is estimated using the laminar-flow result of Hunt (1952):

$$\mu_w = \frac{2k}{b}\sqrt{\frac{\nu}{2\sigma}}\frac{\sinh 2kh}{2kh + \sinh 2kh} \tag{3}$$

where b is the flume width and ν is the kinematic viscosity of the water. The dissipation due to flow through the perforated bottom can be estimated on the basis of a linearized theory for energy loss in oscillatory flow through orifices, but since this still requires empirical values for contraction and loss coefficients, we have used empirical values for μ_p (obtained for waves on still water) in the model-data comparisons shown below.

Dissipation due to Wave Breaking

The rate of wave energy dissipation due to wave breaking is modelled with a modified form of the bore dissipation model by Battjes and Janssen (1978), according to which the power dissipated per unit span in a wave with height H breaking in shallow water of mean depth h is approximated as

$$D' \sim \frac{1}{4}\rho g(\beta' H)^3\sqrt{\frac{g}{h}}, \tag{4}$$

where $\beta' H$ is the height of the foam region in a (spilling) breaker. For saturated breakers, $\beta' = 1$. This model was developed for waves breaking on a sloping bottom, due to limiting water depth. In the present case, the waves break on relatively deep water due to limiting wave steepness. Therefore, here we shall use the wave height H as a characteristic vertical length scale instead of the water depth h, and the (linear) finite-depth intrinsic phase speed c instead of $\sqrt{gh}$:

$$D' \sim \frac{1}{4}\rho g(\beta' H)^3\frac{c}{H} \sim \frac{1}{4}\beta'^3\rho g H^2 c \tag{5}$$

A similar adaptation to the shallow-water dissipation approximation was made by Chawla and Kirby (2002), except that they use a transitional expression for the vertical length scale, approaching the depth h in shallow water and the wave length (actually, k^{-1}) in deep water, as compared to our use of the wave height for the latter condition. Expressed in terms of the wave energy density $E = \frac{1}{8}\rho g H^2$, and absorbing the unspecified proportionality factor in the parameter β', this can be written as

$$D' = 2\beta'^3 cE. \tag{6}$$

It follows that the average rate of wave energy dissipation per unit area of bottom, $D_r = D'/\lambda$, where $\lambda = 2\pi c/\sigma$ is the wave length, is given by

$$D_r = \frac{\beta'^3}{\pi}\sigma E = C_{br}\sigma E, \tag{7}$$

where σ is the intrinsic wave frequency and $C_{br} = \beta'^3/\pi$ is a constant.

A criterion for onset of breaking was used as a threshold for the application of Eq. (7) , based on a maximum wave steepness $(ka)_{max} \approx 0.3$, or

$$H_m \approx 0.1\lambda, \tag{8}$$

where H_m is the maximum wave height.

Uniformly-valid Approximation for the Near Field

To model the near-field waves, we follow the heuristic Taylor expansion method of Peregrine and Smith (1979), extended through the addition of a dissipation function. The equation for the one-dimensional wave propagation in the near field, including dissipation, is represented symbolically as

$$\mathcal{G}(\frac{\partial}{\partial t}, \frac{\partial}{\partial x}, x)\phi + \mathcal{F}(\frac{\partial}{\partial t}, \frac{\partial}{\partial x}, x)\phi = 0, \tag{9}$$

where $\mathcal{G}$ and $\mathcal{F}$ are linear operators, representing propagation and dissipation, respectively (to be specified below). For a single harmonic wave $\phi = \hat{\phi}\exp(i\chi)$, where χ is a phase function, given as $\chi = kx - \omega t$, where k is the wave number and ω is the wave frequency relative to the fixed bed, Eq. (9) is identified with its 'Fourier transform' as

$$G(\omega, k, x)\mathbf{a}\exp(i\chi) + F(\omega, k, x)\mathbf{a}\exp(i\chi) = 0, \tag{10}$$

where $G = 0$ is the dispersion equation and $\mathbf{a}$ is a complex wave amplitude. Using a Taylor expansion of the functions G and F with repect to ω, k and x about their values at the caustic $(\omega_0, k_0, x_0 = 0)$, where $G_k = 0$, the equation for the complex wave amplitude $\mathbf{a}$ is given as

$$xG_x\mathbf{a} - \frac{1}{2}G_{kk}\frac{d^2\mathbf{a}}{dx^2} + F\mathbf{a} - iF_k\frac{d\mathbf{a}}{dx} + xF_{\mathbf{x}}\mathbf{a} + \cdots = 0. \tag{11}$$

The functions G and F and their derivatives are evaluated at $(\omega_0, k_0, x_0 = 0)$. Subscripts denote partial derivatives.

In our experiments, the waves are practically in deep water in the blocking region, allowing the use of the deep-water dispersion equation so that $G(\omega, k, x) = (\omega - kU)^2 - gk$, from which it follows that

$$G_x = 2k(kU - \omega)\frac{dU}{dx} = -2k\sigma\frac{dU}{dx} \tag{12}$$

and

$$G_{kk} = 2U^2. \tag{13}$$

In absence of dissipation, $F = 0$, in which case Eq. (11) simplifies to

$$\frac{1}{2}G_{kk}\frac{d^2\mathbf{a}}{dx^2} - xG_x\mathbf{a} = 0, \tag{14}$$

which is the classical Airy equation for waves near a caustic in the absence of dissipation. Because $G_x > 0$ (note that $U < 0$) and $G_{kk} > 0$, the solution is oscillatory for $x \leq 0$ (at the up-wave side) and monotonic for $x > 0$ (at the down-wave side).

Expressions for the Energy Dissipation and Resulting Evolution Equation

To make the dissipation function $F(\omega, k, x)$ explicit, we follow Booij (1981), who modelled dissipation in the mild-slope equation by adding a damping term $C\partial\phi/\partial t$, where $C = D/E$. We therefore identify the dissipation operator $\mathcal{F}$ with $C\partial/\partial t$. For the single harmonic wave as considered above, the function $F(\omega, k, x)$ becomes

$$F(\omega, k, x) = -i\omega C. \tag{15}$$

The actual expression for the damping coefficient C in terms of the wave parameters ω and k, and the water depth h, depends on the dissipation process under consideration. Considering deep water waves (in the vicinity of the blocking point), $C = C(\omega, k)$. Its spatial dependence is incorporated via $k(x)$. The partial derivatives of F with respect to k and x in the (ω, k, x, t) space are, respectively

$$F_k = -i\omega C_k, \tag{16}$$

$$F_x = -i\omega C_x. \tag{17}$$

With $C = C(\omega, k)$, $C_x = 0$, thus $F_x = 0$. By inserting Eqs (15) and (16) into Eq. (11), we finally obtain the evolution equation for the complex wave amplitude $\mathbf{a}(x)$ as

$$\frac{1}{2}G_{kk}\frac{d^2\mathbf{a}}{dx^2} + \omega C_k \frac{d\mathbf{a}}{dx} - (xG_x - i\omega C)\mathbf{a} = 0. \tag{18}$$

The coefficients of the differential equation (18) are evaluated at $(\omega_0, k_0, x_0 = 0)$. Eq. (18) is the equation for the local wave amplitude in the vicinity of the blocking point including dissipation.

The damping coefficient C is given as $C = D/E = (D_b + D_r)/E$, considering the same energy dissipation processes as in the far field. We then find for C_b, pertaining to the total dissipation at the side walls and the perforated bottom:

$$C_b = \frac{D_b}{E} = 2\mu c_{g;0} = \frac{\mu g}{2\omega} \tag{19}$$

and for C_r, pertaining to wave breaking,

$$C_r = \frac{D_r}{E} = C_{br}\sigma_0 = 2C_{br}\omega \tag{20}$$

where the latter equalities, in terms of the constant ω, apply because the left-hand side expressions are to be evaluated at the blocking point and because the waves are assumed to be in deep water there. The corresponding expressions for the dissipation parameter $C_k = \partial C/\partial k$ have been derived from these equations while neglecting the variation of μ and C_{br} with k, with the result:

$$C_{b,k} = \frac{1}{2}\mu g^{-1/2}{k_0}^{-3/2} = \frac{\mu}{16}\frac{g^2}{\omega^3} \tag{21}$$

for dissipation at the side walls and the bottom, and

$$C_{r;k} = C_{br}c_{g;0} = C_{br}\frac{g}{4\omega} \tag{22}$$

for dissipation due to wave breaking.

Match between Far Field and Near Field Approximations

Having established models for the far field and the near field, these need to be matched in a region which we choose just downstream from the blocking point, in a point $x = x_m$ where the reflected waves may be assumed to have been completely dissipated. This point is estimated at a distance δ downstream from the blocking point x_0, in which δ indicates the order of magnitude of the width of the blocking region. Considering this region as a boundary layer, this magnitude is estimated by Trulsen and Mei (1993) as

$$\delta = O(\epsilon^{-2/3}/\overline{k}), \tag{23}$$

where ϵ is a small parameter given as $\epsilon = (\overline{k}L)^{-1/2}$, $\overline{k} = \omega^2/g$ and L is the horizontal length scale of the current ($L \sim U/(dU/dx)$). In the model-data comparison presented below, we have used a best-fit value for the distance of the matching point from the blocking point given by $x_0 - x_m = 1.1(\overline{k}L)^{-1/3}/\overline{k}$.

Given the wave amplitude in the still-water region at the downstream (up-wave) end of the flow section as an initial value, the far field action balance (Eq. 1) can be integrated to yield the amplitude at the matching point. This provides the boundary condition for the second-order amplitude evolution equation for the near field (Eq. 11) on the oscillatory side of the blocking point. The other boundary condition is $\mathbf{a} \to 0$ as $x \to \infty$.

COMPARISON BETWEEN MODEL RESULTS AND EXPERIMENTS: PERIODIC WAVES

We present here a comparison of model results with observations for periodic waves with period $T = 1.1$ s and target wave amplitude in still water $a_0 = 1.0$ cm. The adverse current discharge has a maximum Q_{max} = 0.12 m^3/s, yielding a maximum cross-sectionally averaged flow velocity of 0.55 m/s in the measurement section above the perforated bottom at 0.55 m below still water level. The discharge decreases linearly from its maximum at $x = 23.0$ m to zero at $x = 11.0$ m, so that the gradient of the cross-sectionally averaged flow velocity is $dU/dx = -0.046$(m/s)/m. The predicted blocking point is at $x = x_0 = 20.45$ m and the matching point is at $x = x_m = 19.4$ m. Because the blocking point position was seen to oscillate spatially in the longitudinal direction, apparently as a result of sideband instability (see Chawla and Kirby 1998), observations at a fixed point in fact cover a finite portion of the blocking region. For this reason, the model results presented in Fig. 1 have been spatially averaged over a distance of 40.0 cm in the region $x \geq x_0 - 2\delta$.

Dissipation in the boundary layers at the sidewalls is estimated on the basis of Eq. (3) due to Hunt (1952), but on account of the turbulent mean flow the molecular viscosity has been replaced by a turbulence viscosity given by $\nu_t = 10^{-4}b|U|$. The decay modulus accounting for the perforated bottom was obtained from observations of wave decay on still water ($\mu_p = 0.014$ m^{-1} for these conditions), whereas the breaker saturation parameter was obtained as a fit parameter (β' = 0.35, indicating unsaturated breakers). Breaking-induced dissipation is effective in the near field only since the steepness in the far field does not exceed the adopted critical value $(ak)_{max} = 0.3$.

The predicted pattern of wave amplitude evolution was seen to agree well with the observations, except that it lies somewhat further downstream (up-wave) than the observed one, which is ascribed to nonlinear effects. These would result in a higher current velocity required to block the waves, thus moving the blocking point further upstream. Such (small) mismatch in location does not matter in practice, but if needed a nonlinear wave speed can be used instead of the linear approximation used here. To illustrate the effect without doing the nonlinear calculations, Fig. 1 shows the comparison between modelled and observed magnitude of the wave amplitude for this test, with the predicted pattern shifted 0.5 m in the upstream (down-wave) direction. (This corresponds to 4% larger current velocity, implying a necessary 4% increase in group velocity.) The predicted pattern so shifted agrees very well with the observed pattern. Note that the uniformly-valid approximation resolves the singularity of the wave amplitude at the blocking point, which would occur in the ray approximation that is used in the far field.

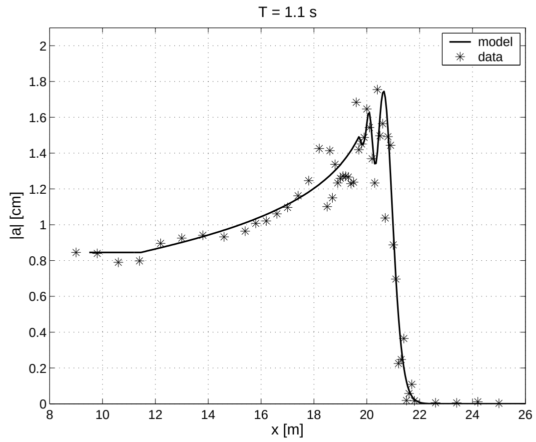

Fig. 1. Modelled (curve) and observed (points) wave amplitude for $T = 1.1$ s, $a_0 = 1.0$ cm. The predicted blocking point is at $x = x_0 = 20.45$ m. The model results have been shifted 0.5 m in the upstream (down-wave) direction.

A MODEL FOR BLOCKING OF RANDOM WAVES

The periodic-wave model described above has been used without essential changes as a basis for a random-wave model, except of course for a translation from a a single frequency to a spectrum.

The linear(ized) dissipation at the sidewalls and at the bottom are estimated per frequency on the basis of Eq. 2, with the spectral energy density $E(\omega)$ now replacing the total energy E. The sidewall dissipation model uses Hunt's frequency-dependent expression Eq. (3) for μ_w as well as a frequency-dependent c_g, with the same turbulence viscosity as in the periodic-wave case, whereas in the case of the bottom perforations we use a frequency-independent $\mu_{p,c}$ and $c_{g,c}$, based on a single characteristic frequency chosen as $\omega_c = m_0/m_{-1}$, in which m_n is the n^{th} moment of the energy spectrum about $\omega = 0$.

The bulk breaking-induced dissipation is based on the Battjes-Janssen (1978) model for random waves:

$$D_{r;tot} = \frac{\alpha}{8\pi} Q_b \sigma_c \rho g H_m^2, \tag{24}$$

where α is a coefficient of order 1, σ_c is a characteristic intrinsic wave frequency, corresponding to ω_c defined above, H_m is the nominal maximum wave height given by

$$H_m = \frac{\gamma}{k_c}, \tag{25}$$

where γ is a breaking parameter and k_c is a characteristic wave number, and Q_b is the probability that a wave height is associated with a breaking or broken wave:

$$\frac{1 - Q_b}{\ln Q_b} = -(\frac{H_{rms}}{H_m})^2, \tag{26}$$

in which H_{rms} is the root mean square wave height. Following Eldeberky and Battjes (1996), the bulk dissipation rate $D_{r;tot}$ is spectrally distributed in proportion to the spectral density to obtain $D_r(\omega)$.

The far-field model is based on the action balance Eq. (1), with c_g, E and D now frequency-dependent. To obtain the near-field model, the energy spectrum $E_{\eta\eta}(\omega)$ at the matching point is discretized into bins of width $\Delta\omega$, from which amplitudes at the matching point are estimated according to

$$\frac{1}{2}a_j^2 \simeq E_{\eta\eta}(\omega_j)\Delta\omega. \tag{27}$$

The near-field amplitude evolution model derived for periodic waves is applied to this discrete set of spectral amplitudes to obtain their local values in the near field, after which Eq. (27) is applied to estimate the local energy spectrum.

COMPARISON BETWEEN MODEL RESULTS AND EXPERIMENTS: RANDOM WAVES

In this section we compare model results with the observations. We consider both partial and (nominally) complete blocking tests. The initial spectrum is of JONSWAP-type with peak period T_p = 1.1 s and significant wave height H_{s0} = 4.0 cm. The maximum current discharge is Q_{max} = 0.078 m^{3}s^{-1} for the partial blocking test and Q_{max} = 0.12 m^{3}s^{-1} for the (nominally) complete blocking test. Going upstream from $x = 25$ m, the flow cross-section gradually widens from 0.4 m in the reduced measurement cross sections to the full flume width of 0.8 m, causing a corresponding decrease in mean flow velocity. This has been taken into account in the computations. The perforated false bottom in the 12 m-long measurement section is at 0.55 m below the still water level. For the dissipation due to the perforations, the characteristic damping modulus is set at $\mu_{p,c}$ = 0.024 m^{-1}, obtained from experiments with periodic waves on still water with T = 1.1 s and H_0 = 5.0 cm. For the dissipation due to wave breaking, we have used $\alpha = 1.0$ as suggested by Battjes and Janssen (1978). The parameter γ, needed for the breaker height H_m, is a calibration parameter.

Fig. 2 shows a comparison between the observed and modelled $H_{m0} = 4\sqrt{m_0}$ and mean zero-crossing period $T_z = \sqrt{m_0/m_2}$ along the flume for the partial blocking case, using $\gamma = 0.30$. It shows a fairly good agreement between the modelled and the observed wave heights, both with respect to the dominant blocking range and the transmitted wave height. The longitudinal variation of the mean zero-crossing period T_z is well predicted, except for a small deviation in the blocking region.

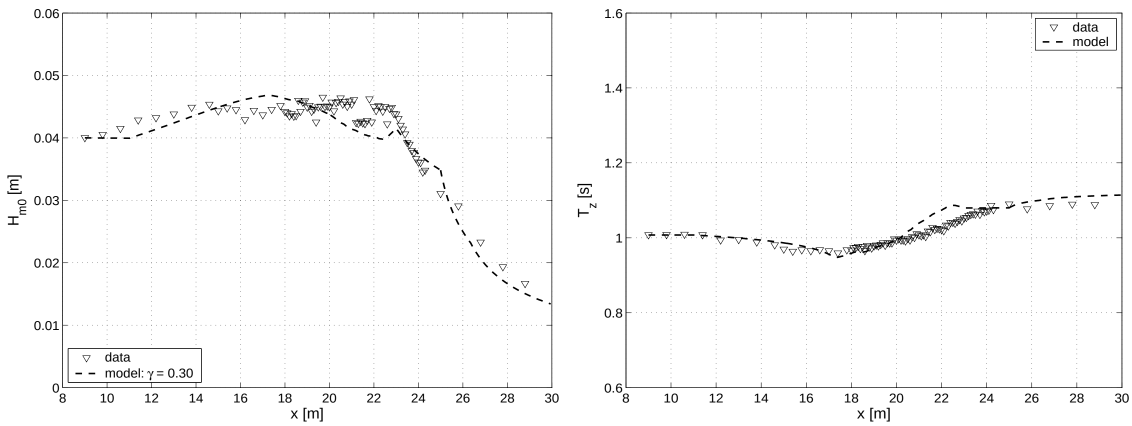

Fig. 2. Comparison between observed (triangles) and modelled (dashed curve) H_{m0} (left panel) and T_z (right panel) for a case of partial blocking; $\gamma = 0.30$.

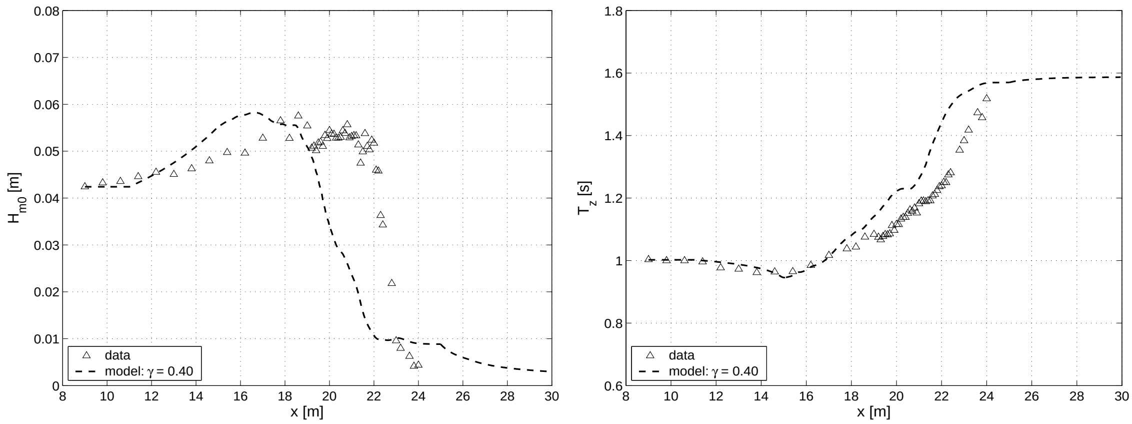

Fig. 3. Comparison between observed (triangles) and modelled (dashed curve) H_{m0} **(left panel) and** T_z **(right panel) for a case of complete blocking;** $\gamma = 0.40$**.**

Similar results for the case of complete blocking are shown in Fig. 3, for $\gamma = 0.40$. The patterns are only fairly well predicted, but the position of the blocking range is grossly misrepresented. Just as in the case of the periodic waves, it is predicted too far up-wave, but in this case the discrepancy is too large to be explained by a nonlinear group velocity correction of a few %. Also, the wave height gradient across the blocking region is underpredicted. We have no satisfactory explanation for these discrepancies, given the fact of a far smaller mismatch in wave height gradient and in position in the cases of periodic waves or partially blocked random waves.

CONCLUSIONS

The experimental and modelling study of wave blocking described above gives rise to the following conclusions.

A novel experimental layout was used in order to eliminate unwanted geometric effects on the waves due to variable depth or width, which occur in conventional arrangements. Instead, the measurement cross-section was held constant and the discharge was varied by distributed suction through a perforated false bottom. The system worked to satisfaction except that it induces additional damping, more than had been anticipated, even for waves that are normally considered in relatively deep water.

A model for the wave propagation was developed accounting for the effects of the non-uniform counter current, consisting of a wave action balance for the slowly varying waves in the approach to the blocking point, which was matched to a caustic-type model for the rapidly varying waves in the blocking region. Dissipation in the boundary layers at the sidewalls, at the perforated bottom and due to breaking was included in the model. One variant of the model is for periodic waves, the other for random waves. In the latter case blocking may be complete or partial, depending on the low-frequency cut-off in the spectrum and the maximum counter current velocity.

The predictive capability of the model was fairly good in case of periodic waves as well as partially blocked random waves, apart from a small spatial shift in the former case. In the case of completely blocked random waves, the overall pattern is only fairly well predicted, and for unknown reasons it is shifted too far up-wave compared to the observations.

The model results referred to above were obtained in part with empirical coefficients as input, mainly in the modelling of various processes of dissipation. A fully predictive model for wave blocking under a variety of conditions is at present still out of reach.

ACKNOWLEDGEMENTS

This research project was financially supported by the Technology Foundation STW, The Netherlands

REFERENCES

Battjes, J.A. and Janssen, J.P.F.M. 1978. Energy loss and set-up due to breaking of random waves. *Proc. 16th Int'l Conf. Coastal Engg.*, Hamburg, 569-587.

Booij, N. 1981. *Gravity waves on water with non-uniform depth and current*. PhD-thesis, Delft University of Technology, The Netherlands.

Chawla, A. and Kirby, T. 1998. Experimental study of wave breaking and blocking on opposing currents. *Proc. 26th Int'l Conf. Coastal Engg.*, 759-772.

Chawla, A. and Kirby, T. 2002. Monochromatic and random wave breaking at blocking points. *J. Geophys. Res. 107(C7)*, 4.1-4.19.

Eldeberky, Y. and Battjes, J.A. 1996. Spectral modelling of wave breaking: application to Boussinesq equations. *J. Geophys. Res. 101(C1)*, 1253-1264.

Hunt, J.N. 1952. Viscous damping of waves over an inclined bed in a channel of constant width. *La Houille Blanche*, 836-842.

Peregrine, D.H. and Smith, R. 1979. Nonlinear effects upon waves near caustics. *Phil. Trans. Roy. Soc. London A 292*, 341-370.

Smith, R. 1975. The reflection of short gravity waves on a nonuniform current. *Math. Proc. Phil. Soc.*, 517-525.

Suastika, I.K. , de Jong, M.P.C. and Battjes, J.A. 2000. Experimental study of wave blocking. *Proc. 27th Int'l Conf. Coastal Engg.*, 227-240.

Trulsen, K. and Mei, C.C. 1993. Double reflection of capillary/gravity waves by a non-uniform current: a boundary layer theory. *J. Fluid Mech. 251*, 239-271.